Grid-scale fluctuations and forecast error in wind power

2016 New J. Phys. 18 023015

(http://iopscience.iop.org/1367-2630/18/2/023015)

New Journal of Physics
The open access journal at the forefront of physics

Deutsche Physikalische Gesellschaft DPG
IOP Institute of Physics

Published in partnership with: Deutsche Physikalische Gesellschaft and the Institute of Physics

OPEN ACCESS

RECEIVED
18 September 2015

REVISED
15 November 2015

ACCEPTED FOR PUBLICATION
4 January 2016

PUBLISHED
1 February 2016

PAPER

Grid-scale fluctuations and forecast error in wind power

G Bel[1], **C P Connaughton**[2], **M Toots**[3] **and M M Bandi**[3]

[1] Department of Solar Energy and Environmental Physics, Blaustein Institutes for Desert Research, Ben-Gurion University of the Negev, Sede Boqer Campus 84990, Israel
[2] Centre for Complexity Science, University of Warwick, Coventry CV4 7AL, UK
[3] Collective Interactions Unit, Okinawa Institute of Science and Technology Onna, Okinawa, 9040495, Japan

E-mail: bandi@oist.jp

Keywords: wind power, correlations, turbulence

Abstract

Wind power fluctuations at the turbine and farm scales are generally not expected to be correlated over large distances. When power from distributed farms feeds the electrical grid, fluctuations from various farms are expected to smooth out. Using data from the Irish grid as a representative example, we analyze wind power fluctuations entering an electrical grid. We find that not only are grid-scale fluctuations temporally correlated up to a day, but they possess a self-similar structure—a signature of long-range correlations in atmospheric turbulence affecting wind power. Using the statistical structure of temporal correlations in fluctuations for generated and forecast power time series, we quantify two types of forecast error: a timescale error (e_τ) that quantifies deviations between the high frequency components of the forecast and generated time series, and a scaling error (e_ζ) that quantifies the degree to which the models fail to predict temporal correlations in the fluctuations for generated power. With no *a priori* knowledge of the forecast models, we suggest a simple memory kernel that reduces both the timescale error (e_τ) and the scaling error (e_ζ).

1. Introduction

Renewable power generation, unlike conventional power, exhibits variability owing to natural fluctuations in the energy source [1], with fluctuation time scales depending on the source type. Whereas biomass and hydroelectric sources vary over long time periods, wind and solar photovoltaics exhibit short time scale variability. Wind power, in particular, shares the spectral features of the turbulent wind from which it derives energy at the scales of an individual turbine [2] and a wind farm [3, 4]. This spectral correspondence implies that correlations of atmospheric turbulence are reflected in the temporal correlations of fluctuations in the generated wind power. One normally assumes that geographically distant wind farms are independent and that temporal correlations in the fluctuating wind power for each farm do not translate into long-range spatial correlations. The total power entering the grid from a large number of distant farms is expected to be much smoother and to exhibit much weaker high frequency fluctuations [5] than the power entering from a single wind farm or a single turbine. This assumption forms the basis for proposals to interconnect local wind farms [6] for the purpose of mitigating wind power fluctuations [5]. Whereas fluctuations do smooth out as an increasing number of wind farms contribute to the aggregate power, it has been shown that the fluctuations are still larger than expected [7].

Using data from the Irish grid operator EIRGRID [8] as a representative example, we studied the temporal correlations in the aggregate wind power entering the Irish grid. The Irish grid is fed by 224 wind farms [9] spread across the Republic of Ireland, a much larger number of farms than the number in the aggregate power previously considered in Texas [7]. We found that the aggregate wind power entering the Irish grid exhibits temporally correlated fluctuations with a self-similar structure. The persistence of correlations, despite an order of magnitude increase in the number of wind farms (and their spatial distribution), strongly points to the presence of long-range spatial correlations in the atmospheric turbulence, which couples geographically distributed wind farms, thereby rendering them non-independent. These results accord with prior studies establishing the presence of long-range correlations within the mesoscale (~1–1000 km) of atmospheric

turbulence [10]. For long time scales, these fluctuations in atmospheric flows were shown to exhibit a multi-fractal structure [11].

Variability adds a cost to renewable power [12, 13] that is absent in conventional power generation. Since an electrical grid has no storage capacity, the production and consumer demand must be balanced in real time at every instant. The grid operator purchases energy units from the producer[4], in an energy market, from a few days to a few milliseconds in advance of delivery. With conventional energy, the grid operator must estimate in advance the consumer demand (scheduling), the estimation of which may not be trivial, and additional energy units required on standby (operating reserves). In the case of renewable energy, the operator must additionally account for both variability (fluctuations) and forecast uncertainty (error) at the production end, calling for uncertainty management [14] in scheduling. Furthermore, large ramps in power fluctuations, in the case of renewable energy, present the possibility of grid destabilization [15] and blackout, a constant source of concern for grid operators [5, 16]. This risk further increases the cost of the operating reserves [17] needed on standby to prevent grid failure [18]. Naturally, forecast models constitute essential tools in estimating the magnitude of fluctuations beforehand and in planning for the optimal operating reserves required on call. Yet, no standards for forecast accuracy currently exist [19].

The performance of a model is often quantified by the mean and variance of the error (deviation of the prediction from the measured value). Extant works on wind power forecast error, ranging from the turbine to the grid scale, have focused on modeling the forecast error distribution [20–25]. Since a probability distribution is time-independent, it contains no information on temporal error variations. Several studies have considered the dependence of the mean and variance of the error on the duration for which the power is predicted (ranging from minutes to hours) [26, 27]. Other works have considered the different distributions of errors for mean power over different durations[5] [22, 23]. However, none of these studies account for the fluctuation correlations of the atmospheric turbulence [28] transferred to the generated power in the analysis of forecast error or for the temporal correlations in the fluctuations and errors themselves. Here, we suggest that the performance of wind power forecast models (as well as the performance of any model for non-stationary processes) should also account for the quality of the prediction against temporal correlations.

To analyze temporal correlations in grid-scale fluctuations for wind power, we draw upon the Statistical Theory of Hydrodynamic Turbulence to quantify two types of forecast error. The first is a timescale error (e_τ) that quantifies the timescales over which the forecast models fail to predict high frequency power fluctuations. This timescale error sets a bound on the numerical resolution of forecast models and would already be known to producers who own the farms and run the forecast models. However, model details are usually not available to grid operators (see footnote 1, [29]) who manage the supply side uncertainty [14]. The second type of error we quantify is a scaling error (e_ζ) that establishes a difference in the self-similar scaling of fluctuations as observed for actual generated power vis à vis the power that was forecast to be generated. This error could be potentially useful to model developers, and if such an error results from large-scale correlations in atmospheric turbulence, incorporating these correlations into models is not subject to limitations arising from numerical resolution. Having established the errors, we employ a simple memory kernel upon the forecast time series and show that the errors are easily reduced with a minimal computational cost.

Two raw time series are provided by EIRGRID: the wind power generated nationwide across all Ireland entering the grid $p_g(t)$, and the power forecast by EIRGRID's models $p_f(t)$ for the same period. The forecast is provided for 24 h at a time (implying different lead times for different times in the forecast series) and is based on a multi-scheme ensemble of regional weather forecast models [30, 31]. The time series sampled at 15 min intervals span a five-year period (2009–2014). As we discuss in the following, we observed no change in the forecast accuracy during this five-year period. Given that most spot markets[6] do not trade at time scales shorter than 15 min [32], our analysis finds potential applicability in these markets, as well as in managing uncertainty over a future horizon of several hours up to a day to improve forecast models.

Raw time series for the generated power $p_g(t)$, forecast power $p_f(t)$, and their instantaneous difference $p_d(t) \equiv p_f(t) - p_g(t)$, which we define as the instantaneous forecast error, are shown in figure 1(a) for a 10 d period, permitting a few immediate qualitative observations. Firstly, $p_g(t)$ exhibits correlated fluctuations. Secondly, $p_f(t)$ while closely following $p_g(t)$, misses the high frequency (relative to the sampling rate of the time series) components. The instantaneous forecast error $P_d(t)$ exhibits correlated fluctuations and its kurtosis $\kappa \equiv \mu_4/\sigma^4 \approx 5.8$ ($\mu_4 \equiv \overline{(p_d - \overline{p_d})^4}$, $\sigma^2 \equiv \overline{(p_d - \overline{p_d})^2}$, and $\overline{p_d}$ represents the time average of the instantaneous error), implying a broader than Gaussian distribution ($\kappa = 3$ for a Gaussian distribution) of the instantaneous error as is evident from figure 1(b).

[4] For Ireland, EIRGRID is both the producer and distributor of wind power.

[5] Note that [22] suggests the Cauchy distribution for the errors. However, this distribution is not suitable because all its moments are undefined [47].

[6] This does not apply for Ireland since its grid is isolated from mainland Europe.

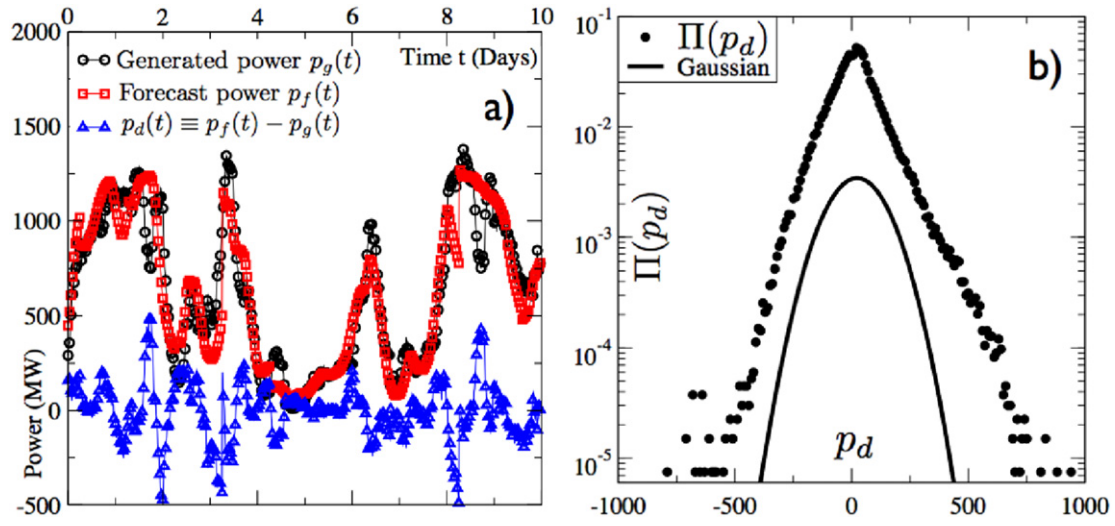

Figure 1. (a) Raw time series (for 10 d) of the generated power $p_g(t)$ (black empty circles), forecast power $p_f(t)$ (red empty squares), and the instantaneous forecast error $p_d(t)$ (blue empty triangles) in megawatts (MW). Every third data point is plotted for easy visibility. (b) The probability density function of the raw instantaneous forecast error $\Pi(p_d)$ (black full circles) has exponentially decaying tails that are broad relative to a Gaussian distribution (solid black line) of the same mean and standard deviation as $\Pi(p_d)$. The Gaussian distribution is vertically shifted for easy comparison.

2. Data analysis

The time series were analyzed in two stages, with trends in the series being identified in the first stage, followed by an analysis of the fluctuations around the trends in the second stage. Trend removal permits a focus on systematic differences between $p_g(t)$ and $p_f(t)$ ignoring differences due to new wind farms and the seasonal variability of the wind power. The trend identification employed here is based on a fast Fourier transform (FFT) analysis of the time series. FFTs of the generated and forecast power time series were obtained, and the frequencies were ranked by their amplitudes (large to small, for each series separately). New time series were obtained by inverting the FFTs, keeping only the first m frequencies (those with the largest amplitudes) and setting the amplitudes of all other frequencies to zero (the amplitudes of the zero frequency components were unchanged in order to preserve the signal mean in the trends). The trends were defined as the time series (obtained by the procedure described above) such that the cross-correlation between the series obtained from the generated and forecast power is maximal. Keeping the original amplitudes of the zero frequency (to preserve the signal mean) and five more frequencies resulted in a peak cross-correlation of 0.9904 between the generated and forecast power trends (figure 2(a)). These respective trends were subtracted from the raw time series. We denote the detrended generated power by $P_G(t)$, forecast power by $P_F(t)$ and their instantaneous difference by $P_D(t) \equiv P_F(t) - P_G(t)$. The frequencies with the maximal amplitudes that were used in the trends correspond to periods of 231–1389 d, implying that the high frequency fluctuations were not affected by our detrending procedure. We emphasize that within the aforementioned protocol, the diurnal oscillation frequency was not explicitly removed from the time series (we elaborate on this point in section 5.).

The characteristic fluctuation timescales for the detrended time series were first computed from their respective autocorrelation functions defined as:

$$C_X(\tau) = \frac{\overline{(P_X(t) - \overline{P_X})(P_X(t+\tau) - \overline{P_X})}}{\overline{(P_X(t) - \overline{P_X})^2}}, \quad (1)$$

where $\overline{P_X}$ is a time-average subtracted from the signal (our detrending renders a zero signal mean since the zero frequency component was preserved in the trend and removed from the detrended series). The subscript X should be replaced with G for generated power, F for forecast power, and D for instantaneous forecast error, respectively. The three autocorrelation functions (figure 2(b)) exhibit exponential decay for short times with a data fit following the functional form $C_X(\tau) \sim A_X e^{-(\tau/\tau_X)}$, where $A_X \simeq 1.0$, owing to $C_X(\tau)$ being normalized, and τ_X represents the characteristic decorrelation time for each time series, yielding $\tau_G = 80.94$ data points (~20.24 h) for generated power, $\tau_F = 81$ points (also ~20.24 h) for forecast power, and $\tau_D = 25.86$ points (~6.5 h) for instantaneous forecast error. Different detrending schemes, i.e., using different numbers of frequencies in the trend (the parameter m defined above), resulted in decorrelation times in the range of 19.5–28 h. However, we found that for all the values of m that we tested, $\tau_F \simeq \tau_G$ and the same trend of a shorter decorrelation time for larger m was found in both the detrended generated and the forecast power. This trend is

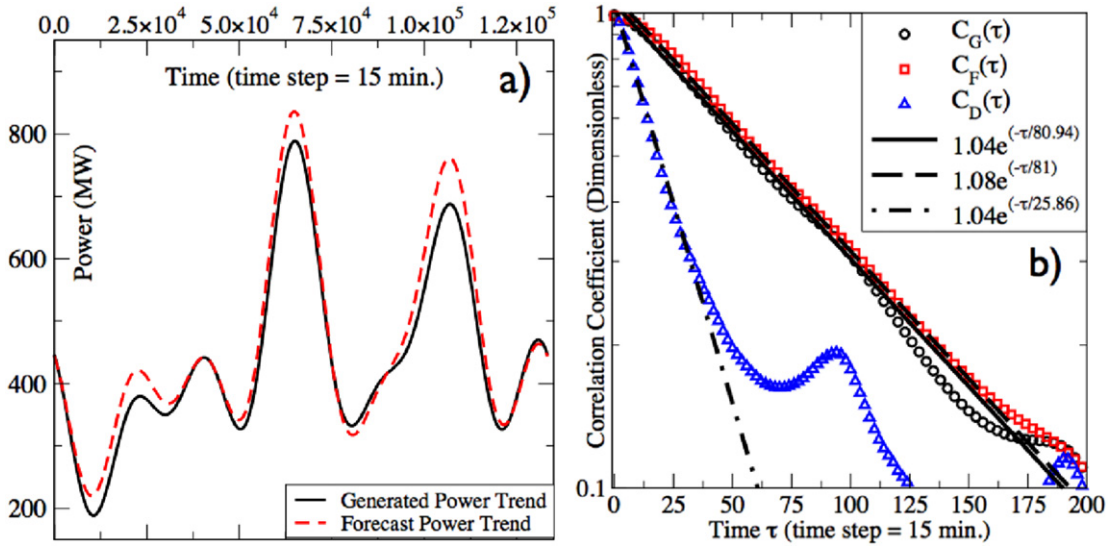

Figure 2. (a) The five-year trends for $p_g(t)$ (solid black line) and $P_f(t)$ (dashed red line) are subtracted from the raw time series in subsequent analysis. (b) Log-linear scale: autocorrelation functions $C_G(\tau)$ (empty black circles), $C_F(\tau)$ (empty red squares) and $C_D(\tau)$ (empty blue triangles) for $P_g(t)$, $P_F(t)$ and $P_D(t)$, respectively, exhibit exponential decorrelation with respective characteristic timescales obtained from the fit to data of $\tau_G = 80.94$ points (20.24 h), $\tau_F = 81$ points (20.24 h) and $\tau_D = 25.86$ points (~6.5 h). Every third data point is plotted for easy visibility.

expected because the larger the m, the larger the deterministic fraction of the signal that is removed in the detrending procedure. The shortest decorrelation time reflects the inherent nature of the fluctuations. The detrended series were also split into independent time series of shorter duration (1/8th of the original temporal duration). Autocorrelation functions computed for these windowed data did not reveal a measurable difference in the characteristic decay time τ_X; deviations were apparent only for long-term behavior, spanning a week (or longer timescales), when the decorrelation had already occurred. The correlation time of high frequency fluctuations ($\lesssim$20 h) is much shorter than the slow varying trend (over months to years). Hence the detrending protocol (in particular, the number of maximal amplitudes) does not influence the analysis to follow-a fact verified and reported upon later. Analysis of the instantaneous forecast error $P_D(t)$ for the eight independent time series of shorter duration did not reveal a measurable change in the fluctuations (mean and standard deviation), suggesting that the forecast accuracy remained the same over the considered five-year period.

Autocorrelation functions for the generated ($C_G(\tau)$) and forecast ($C_F(\tau)$) power exhibit nearly identical scaling and the same characteristic decay timescales ($\tau_G = \tau_F = 20.24$ h), suggesting the accurate capture of correlations in generated power by the forecast models. Yet, the autocorrelation function $C_D(\tau)$ for instantaneous forecast error $P_D(t)$ informs us that some correlations are not captured. In particular, we qualitatively know that $P_F(t)$ misses the high frequency components of $P_G(t)$, and they end up in $P_D(t)$, thereby contributing to its two-point correlator. This correlation deficit suggests that the higher order moments of the two-point correlator are necessary to capture the statistical structure of the missing fluctuations.

3. Temporal structure functions

Statistical analysis of higher order correlations is a well-developed, mature tool within the statistical theory of hydrodynamic turbulence in which higher order two-point correlators are studied through *structure functions*. Kolmogorov's theory of 1941 (K41) [33] lays the foundation for structure functions through the celebrated '4/5 law': $S_3(r) \equiv \langle(\Delta v_{||}(r))^3\rangle \equiv \langle(v_{||}(R+r) - v_{||}(R))^3\rangle = -\frac{4}{5}\bar{\varepsilon}r$, where the third moment of longitudinal velocity differences ($\langle(\Delta v_{||}(r))^3\rangle$) between two points spatially separated by a longitudinal distance r is proportional to the product of the average turbulent dissipation rate ($\bar{\varepsilon}$) and the longitudinal spacing r [34].

The nth order structure function encodes all cross-terms up to order n of the two-point correlator for a given stationary signal. The physical relevance of structure functions may be appreciated by considering a stationary, fluctuating signal $x(t)$ with a zero mean. The difference between two values of this signal taken time τ apart ($\Delta x(\tau) \equiv x(t+\tau) - x(t)$) is collected at various windows (of duration τ) along the time series. $\Delta x(\tau)$ is therefore a random variable with statistics of its own, and the nth order structure function, defined as $S_n(\tau) = \langle(\Delta x(\tau))^n\rangle$, is the nth moment for its probability density function (PDF) $\Pi(\Delta x(\tau))$. The moment

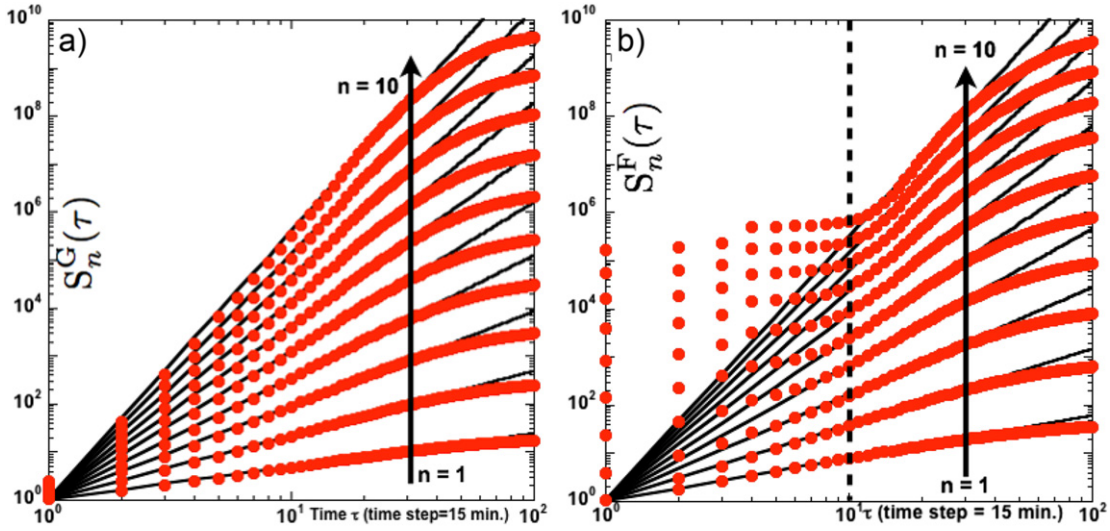

Figure 3. Structure functions of order $n = 1$–10 (solid red circles) and their power-law fits (solid black lines) for (a) generated power $S_n^G(\tau)$ and (b) forecast power $S_n^F(\tau)$ plotted versus τ in log–log scale exhibiting self-similar scaling $S_n^X(\tau) \propto \tau^{\zeta_n^X}$ (X is G for generated and F for forecast power). The scaling is robust for (a) the generated power over 1.4 decades (40 time steps). (b) In contrast, for forecast power, the first- and second-order structure functions exhibit scaling up to $\tau = 40$ time steps, but for $n > 2$, no scaling is observed for $\tau \leqslant 10$ time steps. Self-similar scaling is restored over a limited range of timescales $10 < \tau < 40$.

$S_n(\tau)$ varies with the time difference τ between signals, and its scaling, if any, reveals temporal variations in the statistical structure of the fluctuations of the signal to the nth order.

Tails of the PDF $\Pi(\Delta x(\tau))$ exert themselves with increasing order n of the structure function, thus necessitating more data to resolve higher order structure functions. A weak test for resolving the nth order structure function involves splitting the time series into smaller windows and testing for identical scaling on the truncated series. However, this test only ensures the stationarity of the statistics. A strong test for the ability to resolve the nth order structure function requires that first, the moment's integrand $(\Delta x)^n \Pi(\Delta x) \rightarrow 0$ as $|\Delta x| \rightarrow \infty$ [35] (required due to the finiteness of the data), and second, the PDF $\Pi(\Delta x)$ should decay faster than $1/|\Delta x|^{n+1}$ for $|\Delta x| \rightarrow \infty$ or else the integral $\int (\Delta x)^n \Pi(\Delta x)\ \mathrm{d}x$ would diverge for large $|\Delta x|$ [36] (test for the existence of a PDF's nth moment).Whereas the two conditions are not independent, the second condition is theoretical and does not depend upon the available statistics. When conducting data analysis, even when the second condition is satisfied, insufficient data can lead to noise and prevent the integrand $(\Delta x)^n \Pi(\Delta x)$ from satisfactorily converging to zero [37]. The first condition is, therefore, dependent on the finiteness of the data. Based on both weak and strong tests, we conclude that the EIRGRID data can resolve structure functions up to order $n = 12$; however, we only present results up to $n = 10$. For $n \geqslant 10$, tails of the integrand $(\Delta x)^n \Pi(\Delta x)$ become noisy. Despite the convergence of the integral, the noise amplitude begins to compromise the quality of the structure functions (e.g. please see figure 4 in [38] and related discussion therein) as can be observed in figure 3(a) for $n = 10$.

Since even-order structure functions take only positive values, they converge faster than ones with odd order. To overcome this distinction between odd and even orders, we compute the nth order structure function of the absolute value of differences: $S_n^X(\tau) \equiv \langle |P_X(t+\tau) - P_X(t)|^n \rangle$, where subtraction of mean $\overline{P_X(t+\tau)}$ and $\overline{P_X(t)}$ is assumed. While ensuring the same convergence rate for even- and odd-order statistics, it also collates all data in the positive quadrant, permitting easy visualization.

4. Results

Figure 3 plots the structure functions of order $n = 1$–10 for the absolute value of the signal differences of the generated power $|\Delta(P_G(\tau))|$ (figure 3(a)) and the forecast power $|\Delta(P_F(\tau))|$ (figure 3(b)). Self-similar or power-law scaling is observed for the generated power structure functions over 1.4 decades spanning $\tau \leqslant 40$. Scaling over the same temporal range is also observed for the forecast power structure functions of order $n = 1$ and 2. For $n > 2$, no scaling is observed for timescales $\tau \leqslant 10$. The scaling is restored over a limited range of timescales $10 < \tau < 40$ (0.4 decades in time).

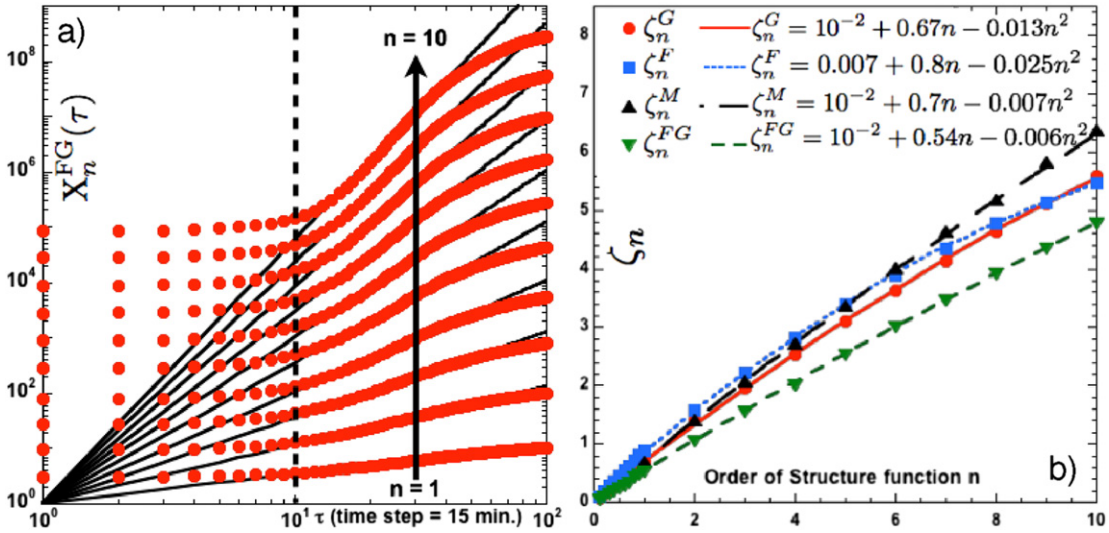

Figure 4. (a) Log–log scale: cross-structure functions $X_n^{FG}(\tau)$ versus τ (solid red circles) exhibit no scaling at early times $\tau \leqslant 10$, with scaling restored for $10 < \tau < 40$. Solid black lines are power-law fits to data within the scaling regime. (b) Scaling exponent ζ_n^X versus the order of structure function n for generated G (solid red circles), forecast F (solid blue squares) and modified forecast M (solid black triangles) structure functions, and cross-structure functions FG (solid green inverted triangles), and their respective second-order polynomial fits: solid red line for ζ_n^G, small dashed blue line for ζ_n^F, long dashed black line for ζ_n^M and medium dashed green line for ζ_n^{FG}.

Self-similar scaling of the temporal structure functions implies a relationship of the form:

$$S_n^X(\tau) \propto A_n^X \tau^{\zeta_n^X}, \tag{2}$$

where ζ_n^X is the scaling exponent. For simple mono-fractal scaling, $\zeta_n^X \propto n$. However, fluctuations with a multi-fractal character exhibit a nonlinear dependence of the scaling exponent ζ_n^X with respect to n. Super- (sub-) linear variation of ζ_n^X versus n implies the temporal expansion (compression) of fluctuations [39]. Scaling exponents for all the structure functions were computed from the log derivative, $\zeta_n^X = \frac{d \log(S_n^X(\tau))}{d \log(\tau)}$, which provides a more reliable estimate of the exponent than a power-law fit [40, 41]. The pre-factor A_n^X in equation 2 is subsequently obtained from a fit to the data. In figure 3, all the data (solid red circles) were divided by A_n^X such that all fits (solid black lines) commence from both mantissa (τ) and ordinate ($S_n^X(\tau)$) at unity, for an easy comparison of ζ_n^X with order n. All the data in figures 3, 4(a) and 5(b), therefore, follow the scaling relation: $S_n^X(\tau) \propto \tau^{\zeta_n^X}$ ($A_n^X \equiv 1$).

The scaling in figure 3 reveals higher order temporal correlations at work in the EIRGRID data. The absence of scaling for $S_n^F(\tau)$ for $n > 2$ at timescales $\tau \leqslant 10$ confirms the qualitative observation made in figure 1(a) that forecast models do not capture high frequency fluctuations. More importantly, figure 3(b) ascribes a precise bound on the time ($\tau = 10$, 2.5 h) up to which the high frequency fluctuations are missed. Finally, the scaling presence for $S_n^F(\tau)$, $n = 1, 2$ explains the close agreement between the autocorrelation functions $C_G(\tau)$ and $C_F(\tau)$ and their identical characteristic decay times, τ_G and τ_F, observed in figure 2(b). This is to be expected on the grounds that the second-order structure function $S_2(\tau) \equiv \langle(\Delta x(\tau))^2\rangle = \langle x(t+\tau)^2\rangle + \langle x(t)^2\rangle - 2\langle x(t)x(t+\tau)\rangle$ shares a direct correspondence with the autocorrelation function where the cross-term is identical to the numerator of equation 1. The failure of $S_n^F(\tau)$ for $n > 2$ to capture high frequency fluctuations out to $\tau = 10$ reveals one type of forecast error in the models; we call this the *timescale error* e_τ.

Before proceeding to the second type of error arising from the scaling mismatch, we define the cross-structure function $X_n^{FG}(\tau) \equiv \langle|P_F(t+\tau) - P_G(t)|^n\rangle$. $X_n^{FG}(\tau)$ represents nth order moments for the PDF of the relative magnitude of fluctuations between $P_G(t)$ and $P_F(t+\tau)$, and their cross-terms correspond to higher order two-point cross-correlators between the generated and forecast power. This function is plotted in figure 4(a). Again, we notice that scaling is absent at early times ($\tau \leqslant 10$), and restored at later times ($10 < \tau < 40$). We note that $X_n^{FG}(\tau)$ exhibits no scaling for $n = 1$ and 2, unlike the forecast structure functions (figure 3(b)). Although $S_n^F(\tau)$ exhibits scaling for order $n = 1$ and 2, its exponent $\zeta_n^F \neq \zeta_n^G$; this scaling deficit is reflected in $X_n^{FG}(\tau)$ for $n = 1$ and 2.

The absence of scaling at short timescales ($\tau \leqslant 10$ time steps) in $S_n^F(\tau)$ for order $n > 2$ (figure 3(b)) and $X_n^{FG}(\tau)$ for all orders n (figure 4(a)) could potentially arise from one of two very different mechanisms. If a day-

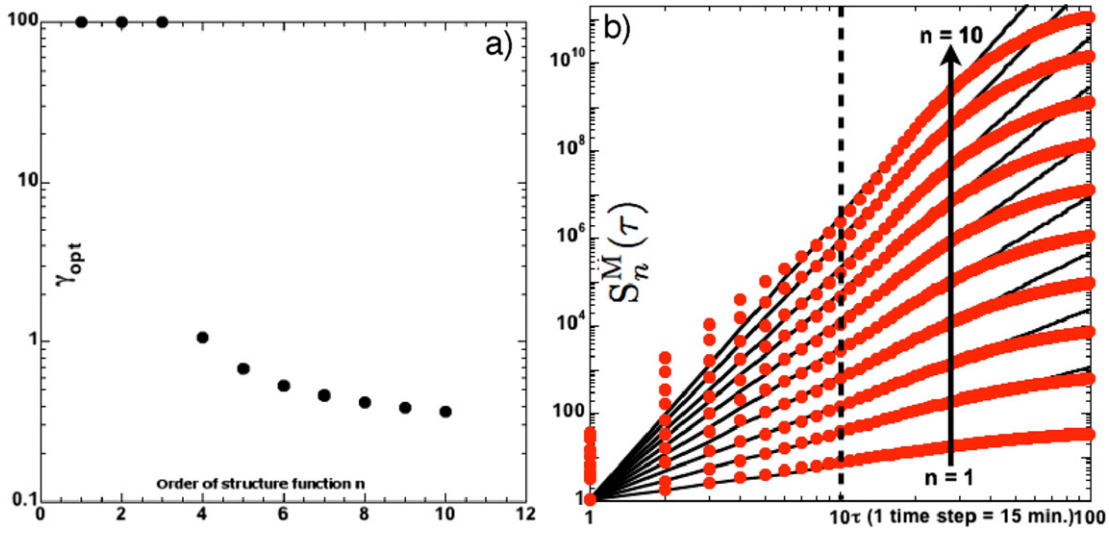

Figure 5. (a) Log-linear scale: γ_{opt} versus order of structure function shows no improvement for $n < 4$ but shows better agreement for $n \geqslant 4$ with an abrupt change observed in γ_{opt} at $n = 4$. (b) Log–log scale: structure functions $S_n^M(\tau)$ versus τ (solid red circles) for the modified forecast time series show considerable improvement over their counterparts $S_n^F(\tau)$ in figure 3(b).

ahead forecast is regularly corrected at short timescales, one expects it will cause short timescale discontinuities in the forecast signal. Owing to these discontinuities, one cannot expect $S_n^F(\tau) \rightarrow 0$ as $\tau \rightarrow 0$, especially for higher order structure functions (large n). EIRGRID generates a day-ahead forecast every calendar day at 00:00 Irish Standard Time (IST) for the next 24 h [30, 31]. A time derivative of the raw (non-detrended) forecast time series $\frac{\partial p_F(t)}{\partial t}$ shows discontinuities only at 24 h intervals (00:00 IST of every calendar day). No short time discontinuities (up to within the sampling interval) were observed. One therefore infers either that EIRGRID does not employ short time corrections or that any such corrections do not exhibit discontinuities in the signal. Consequently, we conclude that short timescale discontinuities make no contribution to higher order structure functions. We, therefore, trace the absence of scaling for $\tau \leqslant 10$ time steps to the second possibility. It must arise from the temporal resolution limitations of the EIRGRID models, including the fact that the boundary conditions for the regional model are only updated every six hours, hence our qualification of this error as a timescale error e_τ.

5. Discussion

Having established the various structure functions, we now consider the behavior of their scaling exponents ζ_n^X ($X \equiv$ G for generated, F for forecast and FG for the cross-structure function). Figure 4(b) plots ζ_n^X versus the order n together with their polynomial fits to the quadratic order. $\zeta_n^G = 10^{-2} + 0.67n - 0.013n^2$ scales almost linearly (mono-fractal) with a small, but measurable, quadratic deviation towards multi-fractal behavior. The exponent $\zeta_n^F = 0.007 + 0.8n - 0.025n^2$ exhibits a slightly more pronounced quadratic deviation (multi-fractal behavior) relative to ζ_n^G. On the other hand, $\zeta_n^{FG} = 10^{-2} + 0.54n - 0.006n^2$ scales almost linearly with n, implying mono-fractal scaling.

We now consider the measurement error for the aforementioned scalings. First, given that all detrending protocols suffer from the ad hoc choice of a detrending timescale, we tested the scalings for dependence on the detrending procedure by varying the number of maximal amplitudes. Ignoring the condition for maximal cross-correlation between $p_g(t)$ and $p_f(t)$, the number of maximal amplitudes contributing to the trends was varied. The scalings were invariant up to the inclusion of 15 maximal amplitudes into the trend, beyond which coefficients for the polynomial fits started varying in the second decimal place.

Contrary to normal practice [19], we did not explicitly detrend the diurnal oscillation frequency as it was found not to be relevant for our analysis. First, we focused on fluctuations for timescales less than 24 h. In particular, we observed self-similar scaling in structure functions up to 10 h ($\tau = 40$ time steps). Since our analysis cannot apply beyond this timescale, diurnal oscillations do not enter into our analysis. Second, whereas diurnal peaks are present in the autocorrelation function (figure 2(b)) for the instantaneous forecast error ($C_D(\tau)$), we did not calculate structure functions for instantaneous forecast error ($P_D(t)$). Diurnal modes are barely discernible for the autocorrelation functions of generated ($C_G(\tau)$) and forecast power ($C_F(\tau)$) whose

structure functions we do study. Finally, as stated earlier, our detrending protocol revealed that diurnal oscillations in the forecast and generated power are less significant than other (much slower) processes.

Having ascertained the robustness of our choice for the five maximal amplitudes at which the cross-correlation peaks, we focused on a second source of scaling measurement error, namely statistical variability. Since the scalings are analyzed up to $\tau = 100$ data points, the detrended time series were split into eight independent windows (each with 21 912 data points), and the structure functions were recomputed for each window. The variation in the log derivative $\left(\zeta_n^{\mathrm{X}} = \frac{d\ \log(S_n^{\mathrm{X}}(\tau))}{d\ \log(\tau)}\right)$ for the eight independent measurements was taken as the possible scatter in the scaling estimation, thereby providing a confidence interval for the polynomial fits. The scatter was found to be $\zeta_n^{\mathrm{X}} \pm 0.01$ in both the measured value of ζ_n^{X} and the corresponding polynomial fits (for each of the polynomial coefficients) for each of the eight independent datasets, revealing that the polynomial fits were meaningful only to the linear order for ζ_n^{G} and ζ_n^{FG}. The quadratic-order polynomial coefficient for ζ_n^{F}, despite being larger than the scatter of ± 0.01, is not useful owing to the fact that the corresponding quadratic terms for ζ_n^{G} and ζ_n^{FG} are smaller than the scatter magnitude.

Despite qualitatively observing a quadratic deviation for ζ_n^{X} in figure 4(b), our inability to ascribe significance to it arises from the fact that the multi-fractal component (deviation from linear scaling) of the scalings is minuscule. This is significant in light of several studies that have demonstrated multi-fractal scaling for wind power fluctuations at the turbine [2, 4] and farm scales [42]. Turbulence theory traces the source of multi-fractal behavior to intermittent fluctuations that can arise from two sources in the atmospheric context. The first, known as internal intermittency, occurs at the small scales of turbulent flow. These intermittent fluctuations would be naturally reflected in the power generated at the turbine and farm scales. However, when adding together power generated by geographically distant wind farms, internal intermittency should smooth out [7] since it is a small-scale effect and cannot extend across geographically distributed wind farms. Furthermore, the sampling interval (15 min) for EIRGRID data is not expected to resolve any effects that may arise from internal intermittency, which occur at much shorter timescales (high frequencies).

The second source of intermittency, known as external intermittency, occurs at the edge of any free-stream [43] and arises in the atmospheric context due to coupling between the atmospheric boundary layer turbulence and a co-moving weather system [28]. External intermittency, which can be experienced in the form of wind gusts, is of greater relevance in the present analysis as it can both correlate distributed farms through the weather system and occur at timescales longer than the 15 min sampling interval for the EIRGRID data. The nearly fractal scaling of ζ_n^{G} informs us that both internal and external intermittency are being smoothed to the point of rendering grid-level power fluctuations almost mono-fractal.

The self-similar scaling of $S_n^{\mathrm{G}}(\tau)$ over several hours does strongly point to the influence of large-scale turbulent structures on power fluctuations at the grid level. The 20 h characteristic decorrelation time (τ_{G}) for generated power in figure 2(c), if taken as the large eddy turnover time of atmospheric turbulence, also lends credence to such an argument. Finally, independent proof in support of this argument also comes from Katzenstein *et al* [7] who show that an individual wind farm exhibits $f^{-5/3}$ (f being the frequency) scaling for the wind power spectrum (equivalent to $\tau^{2/3}$ scaling of the second-order structure function in the time domain). However, as wind power from various farms is summed, the spectrum steepens (please see figure 3 in [7]). Such spectral steepening can be clearly attributed to the smoothing of high frequency (short timescale) fluctuations corresponding to small eddies. But the low frequency (long timescale) fluctuations corresponding to large-scale eddies lose no power spectral density, clearly indicating the influence of large-scale turbulent structures on wind power. These large eddies extend across great geographic distances to couple distributed wind farms. No longer independent of each other, their fluctuations become correlated, and thus cannot smooth out when summed at the electrical grid. This spatial coupling of wind farms via atmospheric turbulence manifests itself through correlated fluctuations in the aggregate wind power feeding the electrical grid.

We finally consider the forecast error due to the scaling mismatch. We define the scaling error as $e_\zeta \equiv \zeta_n^{\mathrm{F}} - \zeta_n^{\mathrm{G}}$. Under this definition, if the time series for forecast and generated power were identical, then $S_n^{\mathrm{G}}(\tau) \equiv S_n^{\mathrm{F}}(\tau)$, implying $\zeta_n^{\mathrm{G}} \equiv \zeta_n^{\mathrm{F}}$, and therefore $e_\zeta = 0$. Another typical case arises if forecast models fail completely, resulting in a flat time series with no fluctuations, $\zeta_n^{\mathrm{F}} = 0$, resulting in an error $e_\zeta = -\zeta_n^{\mathrm{G}}$. Using the polynomial fits for ζ_n^{X} (see figure 4(b)) to the linear order, we obtain $e_\zeta = (7 \times 10^{-3} + 0.8n) - (10^{-2} + 0.67n) = -0.003 + 0.13n$. This can be cross-validated against the difference $\zeta_n^{G} - \zeta_n^{\mathrm{FG}} = (10^{-2} + 0.67n) - (10^{-2} + 0.54n) = 0.13n$. Since $\zeta_n^{\mathrm{X}} \to 0$ as $n \to 0$, the 0th order term falling within the scatter may be taken to be zero. Both estimates of error are identical to the linear order ($e_\zeta = 0.13n$).

The analysis thus far demonstrates the importance of temporal correlations in wind power and their role in estimating forecast errors. It is reasonable to ask whether this knowledge could help in improving the forecast time series, despite having no knowledge of the models employed. Motivated by the observation that the short-term temporal correlations of the generated power are not well captured by the forecast, we introduce a modified

forecast that is based on the original forecast, convoluted with an exponentially decaying memory kernel derived from the generated power time series. The modified forecast power is given by $P_{\rm M}(t) = \int_0^t P_{\rm F}(\tau)\mathrm{e}^{-\gamma(t-\tau)}\mathrm{d}\tau$. This modified forecast imposes a short-term correlation on the original forecast; therefore, it is expected to better capture the temporally correlated fluctuations of the generated power.

The memory duration $(1/\gamma)$ was chosen so as to minimize the relative difference between the structure functions of the generated and forecast power. As expected (as shown earlier, the low order structure functions of the generated and forecast power are very similar), we found that the optimal γ varies with the order of the structure function. For $n < 4$, the memory-modified forecast shows no improvement in the agreement between $S_n^{\rm G}$ and $S_n^{\rm F}$. For $n \geqslant 4$, the modified forecast exhibits better agreement with the structure functions of the generated power as shown in figure 5(b). The optimal γ ($\gamma_{\rm opt}$) was found to be $\gamma_4 \approx 1.06$ and $\gamma_{10} \approx 0.37$, as shown in figure 5(a), plotted in log-linear scale to show the variation in $\gamma_{\rm opt}$ for $n \geqslant 4$. The simple scheme, suggested here, not only tries to rectify the timescale error e_τ, but also attempts to statistically align the temporal correlations by improving the scaling error e_ζ.

As is apparent from figure 5(b), the structure functions $(S_n^{\rm M}(\tau) \equiv \langle|\Delta P_{\rm M}(\tau)|^n\rangle)$ for modified forecast time series are substantially improved over their unmodified counterpart (figure 3(b)). First, scalings are restored at high frequencies ($\tau \leqslant 10$), thus rendering the timescale error irrelevant. More importantly, the scaling itself is improved as is evident from figure 4(b), revealing $\zeta_n^{\rm M} = 0.01 + 0.7n - 0.007n^2$. To the linear order, the scaling error $e_\zeta = \zeta_n^{\rm M} - \zeta_n^{\rm G} = 0.7n - 0.67n = 0.03n$, a considerable improvement over the original forecast time series. Being computationally inexpensive, and given that spinning and non-spinning reserves must act within 10 min of failure [44], with replacement reserves acting within 20–60 min, there are tangible benefits to incorporating such a memory kernel into models to monitor instabilities in real-time. Furthermore, it might be possible to improve the forecast models using different parameterizations of the regional climate models or weather models, or other stochastic approaches such as Markov-chain-based prediction methods [45]. It is important to note that the improvement in the prediction does not come at the expense of an increase in the error. We verified that for the values of γ (in the memory kernel) that we used, the root mean squared error $(\mathrm{rmse} = \sqrt{\frac{1}{N}\Sigma_{t=1}^{N}(P_{\rm F}(t) - P_{\rm G}(t))^2})$ and the cross-correlation between the modified forecast and the generated power were within 1% of those of the original forecast.

6. Summary

In summary, wind power exhibits significant temporal correlations even at the grid level, where fluctuations are expected to average out [5] as power is fed from geographically distributed wind farms. Previous studies have shown that the temporal correlations of the wind are essential to studying wind-generated large-scale ocean currents [46]; a similar appreciation of large-scale correlations in atmospheric turbulence within the context of wind power is called for. Fluctuations, albeit posing a problem to system operators, possess a statistical structure through temporal correlations, which could be exploited to quantitatively analyze the error in forecast models. The technique proposed here is only limited by the sampling rate of the time series. Beyond potentially serving as a standard for quantifying wind-power forecast accuracy, it could have applications for any renewable energy source with temporally correlated fluctuations possessing a statistical structure.

Acknowledgments

MT and MMB were supported by the Collective Interactions Unit at the Okinawa Institute of Science and Technology Graduate University. CPC was hosted by the Collective Interactions Unit at the Okinawa Institute of Science and Technology Graduate University while performing this work. GB was supported through the European Union Seventh Framework Programme (FP7/2007-2013) under grant number 293825. The authors gratefully acknowledge EIRGRID for permission to use their data.

References

[1] MacKay D J C 2009 *Sustainable Energy—Without the Hot Air* (Cambridge: UIT Cambridge)
[2] Milan P, Wächter M and Peinke J 2013 *Phys. Rev. Lett.* **110** 138701
[3] Apt J 2007 *J. Power Sources* **169** 369
[4] Calif R, Schmitt F G and Huang Y 2014 *Geophys. Res. Abstr.* **16** 15443
[5] Wiser R, Yang Z, Hand M, Hohmeyer O, Infield D, Jensen P H, Nikolaev V, O'Malley M, Sinden G and Zervos A 2011 Wind energy *IPCC Special Report on Renewable Energy Sources and Climate Change Mitigation* (Cambridge: Cambridge University Press)
[6] Jacobson M Z and Delucchi M A 2009 *Sci. Am.* **301** 58
[7] Katzenstein W, Fertig E and Apt J 2010 *Energy Policy* **38** 4400

[8] http://eirgrid.com/operations/systemperformancedata/windgeneration/
[9] Irish Wind Energy Association (http://iwea.com/faqs)
[10] Muzy J F, Baïle R and Poggi P 2010 *Phys. Rev.* E **81** 056308
[11] Lovejoy S, Schertzer D and Stanway J D 2001 *Phys. Rev. Lett.* **86** 5200
[12] Lueken C, Cohen G E and Apt J 2012 *Environ. Sci. Technol.* **46** 9761
[13] Katzenstein W and Apt J 2012 *Energy Policy* **51** 233
[14] Matos M A and Bessa R J 2011 *IEEE Trans. Power Syst.* **26** 594
[15] Tande J O G 2000 *Appl. Energy* **65** 395
[16] Albadi M H and El-Saadany E F 2010 *Electr. Power Syst. Res.* **80** 627
[17] Fabbri A, Gomez San Roman T, Abbad R and Quezada V H M 2005 *IEEE Trans. Power Syst.* **20** 1440
[18] Parsons B P, Milligan M, Zavadil B, Brooks D, Kirby B, Dragoon K and Caldwell J 2004 *Wind Energy* **7** 87
[19] Costa A, Crespo A, Navarro J, Lizcano G, Madsen H and Feitosa E 2008 *Renew. Sustainable Energy Rev.* **12** 1725
[20] Doherty R and O'Malley M 2005 *IEEE Trans. Power Syst.* **20** 587
[21] Bludszuweit H, Dominguez-Navarro J A and Llombart A 2008 *IEEE Trans. Power Syst.* **23** 983
[22] Hodge B M and Milligan M 2011 *NREL Report No.* : NREL/CP-5500-50614
[23] Hodge B M, Ela E G and Milligan M 2012 *Wind Eng.* **23** 509
[24] Hodge B M *et al* 2012 Wind power forecasting error distributions: an international comparison *Tech. Rep* National Renewable Energy Laboratory
[25] Wu J, Zhang B, Li Z, Chen Y and Miao X 2014 *Electr. Power Energy Syst.* **55** 100
[26] Madsen H, Pinson P, Kariniotakis G, Nielsen H A and Nielsen T S 2009 *Wind Eng.* **29** 475
[27] Lange M 2005 *J. Sol. Energy Eng.* **127** 177
[28] Katul G G and Chu C R 1994 *Phys. Fluids* **6** 2480
[29] Weber C 2010 *Energy Policy* **38** 3155
[30] Lang S C, Möhrlen J, Jørgensen B, Gallachóir O and McKeogh E 2006 Forecasting total wind power generation on the republic of ireland grid with a multi-scheme ensemble prediction system *Proc. Global Wind Energy Conf. GWEC Adelaide*
[31] Lang S and McKeogh E 2009 *Wind Eng.* **33** 433–48
[32] German TSO Intraday Market: www.epexspot.com/en/product-info/Intraday/germany
[33] Kolmogorov A N 1941 *Dokl. Akad. Nauk SSSR* **32** 16
[34] Frisch U 1995 *Turbulence: The Legacy of A. N. Kolmogorov* (Cambridge: Cambridge University Press)
[35] Bandi M M, Goldburg W I, Cressman J R and Pumir A 2006 *Phys. Rev.* E **73** 026308
[36] Samorodnitsky G and Taqqu M S 1994 *Stable Non-Gaussian Random Processes* (New York: Chapman and Hill)
[37] Anselmet F, Gagne Y, Hopfinger E J and Antonia R A 1984 *J. Fluid Mech.* **140** 63
[38] Anselmet F and Antonia R A 1984 *J. Fluid Mech.* **140** 63
[39] Mandelbrot B and Hudson R L 2004 *The Misbehaviour of Markets: A Fractal View of Financial Turbulence* (New York: Basic Books)
[40] Chen S Y, Dhruva B, Kurien S, Sreenivasan K R and Taylor M A 2005 *J. Fluid Mech.* **533** 183
[41] Larkin J, Bandi M M, Pumir A and Goldburg W I 2009 *Phys. Rev.* E **80** 066301
[42] Calif R, Schmitt R and Huang Y 2013 *Physica* A **392** 4106
[43] Kuznetsov V R, Praskovsky A A and Sabelnikov V A 1992 *J. Fluid Mech.* **243** 595
[44] Billinton R and Allan R 1996 *Reliability Evaluation of Power Systems* (New York: Plenum)
[45] Pesch T, Schröders S, Allelein H J and Hake J F 2015 *New J. Phys.* **17** 055011
[46] Bel G and Ashkenazy Y 2013 *New J. Phys.* **15** 053024
[47] Lévy P 1954 *Théorie de l'addition des variables aléatoires* (Gauthier Villars: Paris)